a remote site *via* a personal computer and cellular phone. Using these measured physiologic data, it is important to estimate the internal physiologic conditions and the physiologic strategy against the physiologic behaviors for the purpose of controlling the artificial heart to adapt to the physiologic behaviors.

The purpose of this research is to propose a method of estimating the physiologic strategy based on a mathematical model for assisting and substituting for the cardiac functions by the robotic artificial heart using online parameter identification from some measured data, i.e. Aop and blood flow. By estimating the physiologic strategy as the changes in the identified physiologic parameters, it is possible to produce effective medical care and therapeutic control using the robotic artificial heart able to adapt to the physiologic changes.

In Section 2, the systemic circulation is modeled from physical and physiologic knowledge, and the method of estimating the physiologic parameters and resonant frequency using the online parameter identification method with the δ operator is described. In Section 3, the results of the computer simulation study and animal experiments are discussed. Sections 4 and 5 present the discussion and conclusion, respectively.

2. MATERIALS AND METHODS

The method employed estimates the physiologic strategy by the changes of the physiologic parameters in the systemic circulation and the resonant frequency. The physiologic parameters of the systemic circulation are identified from a mathematical model using online parameter identification with the δ operator. The resonant frequency is calculated from the identified physiologic parameters. The outline of this method is shown in Fig. 2.

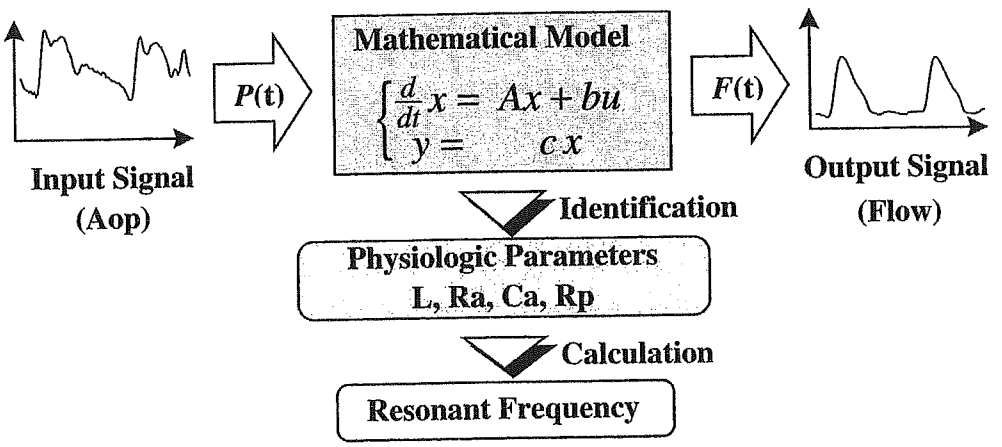

Figure 2. The physiologic strategy can be estimated by the changes in the physiologic parameters of the systemic circulation identified from the mathematical model using parameter identification and the resonant frequency calculated from the identified physiologic parameters.

2.1. Systemic circulation model

In order to observe the immeasurable physiologic parameters that control the hemodynamics of the systemic circulation, many physiologic models have been proposed [9–11]. Although a complex model can be built, it is difficult to identify all of the variable physiologic parameters because of the measurement noise and abbreviated dynamics, etc. Thus, by using a blood vessel model, we adopt a simple model, a second-order physiologic model, represented by the mathematical equations in Fig. 3.

Because blood is an incompressible fluid, Navier–Stokes theory is applied. With regard to the inertia characteristics, we assume that the velocity distribution is flat. With regard to the characteristics of viscosity, we assume that blood flow follows Poiseuille's Law. By applying these theories, the characteristics of the physiologic parameters inertia (L'), resistance (R') and compliance (C') are defined as:

$$L' = \frac{\rho}{\pi r^2}, \quad R' = \frac{8\mu}{\pi r^4}, \quad C' = \frac{2\pi r^3(1-\sigma^2)}{Eh}, \tag{1}$$

where r is the inside diameter of the vessel, E is Young's modulus, h is the thickness of the vessel, σ is Poisson's ratio, ρ is the density of blood and μ is the coefficient of viscosity. These physiologic parameters adjust the hemodynamics and reflect physiologic behavior, i.e. the behavior of the central nervous system.

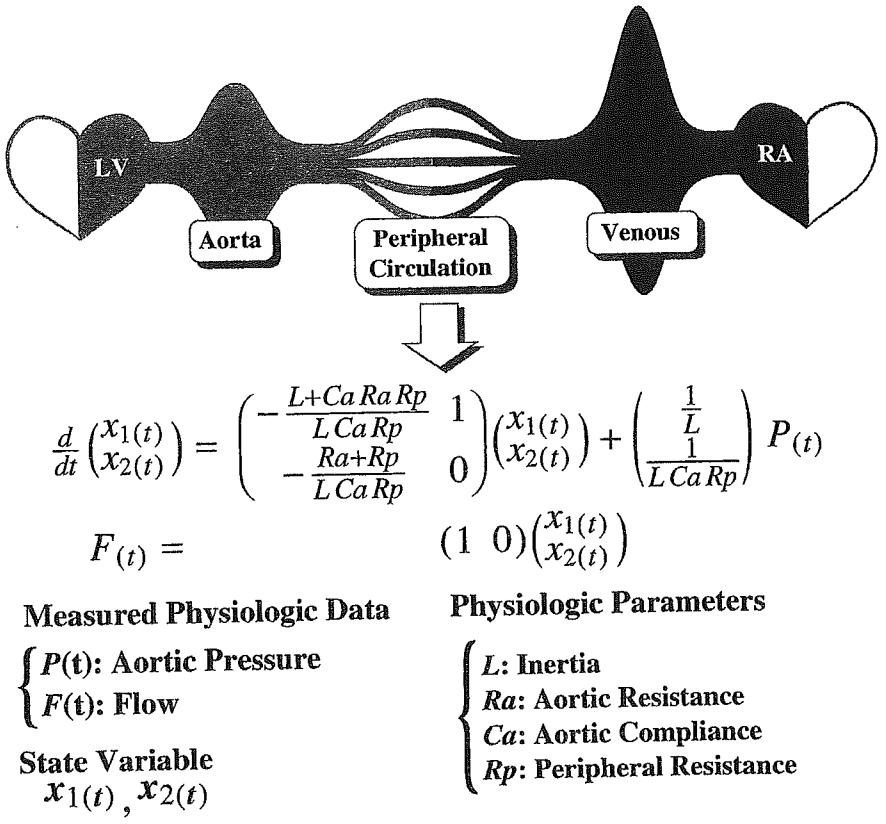

Figure 3. Physiologic model represented by the mathematical equation.

L' corresponds to the mass of blood, R' corresponds to the fluid resistance of the blood vessel and C' corresponds to the elasticity of the blood vessel.

By considering the complex systemic circulation as a linear system and a lumped element circuit, the systemic circulation model, which consists of series aortic inertia (L), aortic resistance (R_a), parallel aortic compliance (C_a) and total peripheral resistance (R_p), is represented by:

$$\begin{cases} \dfrac{d}{dt}\begin{pmatrix} x_{1(t)} \\ x_{2(t)} \end{pmatrix} = \begin{pmatrix} -a_{c1} & 1 \\ -a_{c2} & 0 \end{pmatrix}\begin{pmatrix} x_{1(t)} \\ x_{2(t)} \end{pmatrix} + \begin{pmatrix} b_{c1} \\ b_{c2} \end{pmatrix} P_{(t)} \\ F_{(t)} = (1 \quad 0)\begin{pmatrix} x_{1(t)} \\ x_{2(t)} \end{pmatrix}, \end{cases} \tag{2}$$

where:

$$\begin{cases} a_{c1} = \dfrac{L + C_a R_a R_p}{L C_a R_p}, \quad a_{c2} = \dfrac{R_a + R_p}{L C_a R_p} \\ b_{c1} = \dfrac{1}{L}, \quad b_{c2} = \dfrac{1}{L C_a R_p}. \end{cases}$$

In (2), $P(t)$ is the measured Aop. $F(t)$ is the measured blood flow, and $x_1(t)$ and $x_2(t)$ are state variables.

2.2. *Parameter identification with the δ operator*

In order to identify the physiologic parameters in the model, the system identification method using the δ operator is adopted. The outline of parameter identification is shown in Fig. 4.

First, this model is transformed to the discrete time model for applying online parameter identification. Generally, the shift operator is applied to represent the discrete time model. However, when the sampling time reaches zero, the similarity between the continuous time model and the discrete time model is lost. Therefore, we apply the δ operator [12] as:

$$\delta F(t) = \frac{F(t + T_s) - F(t)}{T_s}, \tag{3}$$

where T_s is the sampling time. It has similarity to the continuous time model when the sampling time reaches zero. By applying the δ operator, the physiologic model is represented as:

$$\delta^2 F_{(t)} = -\delta a_1 F_{(t)} - a_2 F_{(t)} + \delta b_1 P_{(t)} + b_2 P_{(t)}, \tag{4}$$

where:

$$\begin{cases} a_1 = a_{c1}, \quad a_2 = a_{c2} \\ b_1 = \dfrac{1}{2}\{b_{c2} T_s + b_{c1}(2 - a_{c1} T_s)\}, \quad b_2 = b_{c2} - \dfrac{T_s}{2} a_{c2} b_{c1}. \end{cases}$$

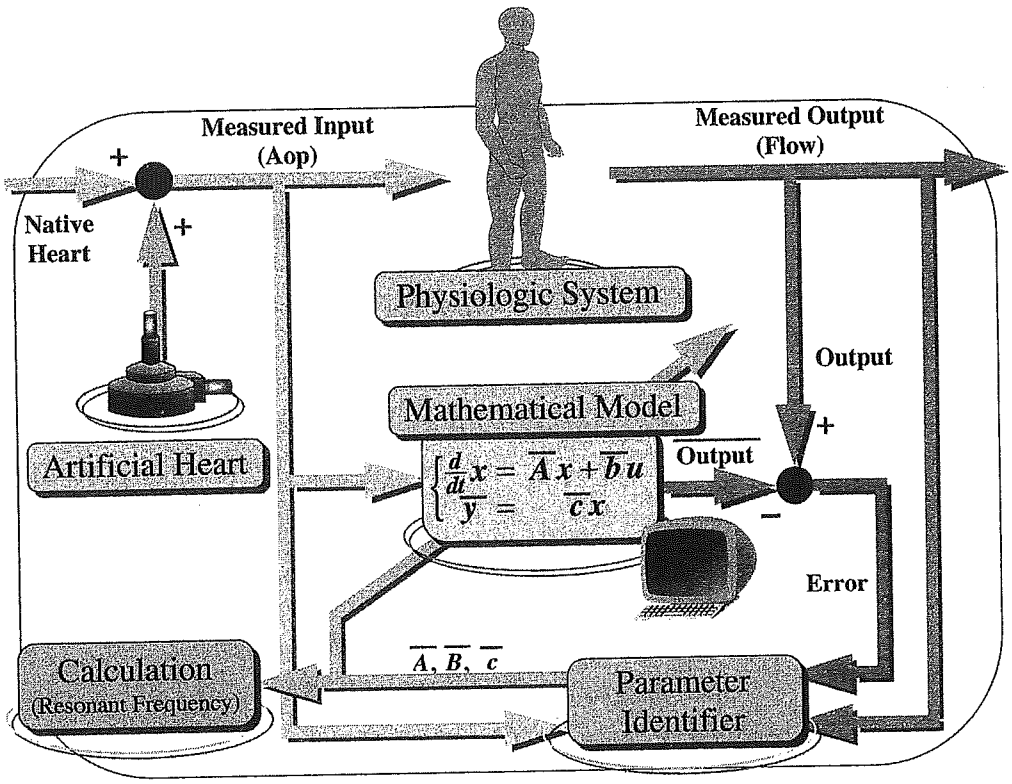

Figure 4. Data processing of the parameter identification.

To eliminate noise, the state variable filter $E(\delta)$ [13] is applied as:

$$E(\delta) = \delta^2 + e_1\delta + e_2, \tag{5}$$

where e_1 and e_2 are decided by the characteristics of this filter. By using the unknown parameter vector θ and the data vector φ, (4) is transformed as:

$$\overline{F(t)} = \varphi(t)^t\theta,$$
$$\varphi(t) = \left[\frac{\delta F(t)}{E(\delta)} \quad \frac{F(t)}{E(\delta)} \quad \frac{\delta P(t)}{E(\delta)} \quad \frac{P(t)}{E(\delta)}\right]^t, \quad \theta = [e_1 - a_1 \quad e_2 - a_2 \quad b_1 \quad b_2]^t, \tag{6}$$

where $\overline{F}(t)$ is the predicted output estimated by the physiologic model. We solve the physiologic parameters that produce the error between the measured output and the predicted output minimum using the online least-squares method as [14]:

$$\delta\theta_{(t)} = \frac{1}{T_s}\frac{D_{(t-1)}\varphi_{(t)}}{1 + \varphi^t_{(t)}D_{(t-1)}\varphi_{(t)}}\left[F(t) - \varphi^t_{(t)}\theta\right],$$
$$\delta D_{(t-1)} = -\frac{1}{T_s}\frac{D_{(t-1)}\varphi_{(t)}\varphi^t_{(t)}D_{(t-1)}}{1 + \varphi^t_{(t)}D_{(t-1)}\varphi_{(t)}}. \tag{7}$$

Using this calculation, the physiologic parameters in the unknown parameter vector θ are identified. Using the parameters a_{c1}, a_{c2}, b_{c1} and b_{c2} in the continuous

time model, the physiologic parameters can be given as:

$$\begin{cases} L = \dfrac{1}{b_{c1}}, \quad R_a = \dfrac{a_{c1}b_{c1} - b_{c2}}{b_{c1}^2} \\ C_a = \dfrac{b_{c1}^3}{a_{c2}b_{c1}^2 - a_{c1}b_{c1}b_{c2} + b_{c2}}, \quad R_p = \dfrac{a_{c2}}{b_{c2}} - \dfrac{a_{c1}}{b_{c1}} + \dfrac{b_{c2}}{b_{c1}^2}. \end{cases} \tag{8}$$

Thus, the physiologic parameters can be identified by (4), (7) and (8).

2.3. *Calculation of resonant frequency*

In order to calculate the resonant frequency, (2) is converted to the impedance equation that can represent the frequency response. The impedance equation $Z(jw)$ is given by:

$$Z_{(jw)} = \frac{P_{(jw)}}{F_{(jw)}} = \frac{(jw)^2 + ja_{r1}w + a_{r2}}{jb_{r1}w + b_{r2}}, \tag{9}$$

where:

$$a_{r1} = \frac{L + R_aR_pC_a}{LR_pC_a}, \quad a_{r2} = \frac{R_a + R_p}{LR_pC_a}, \quad b_{r1} = \frac{1}{L}, \quad b_{r2} = \frac{1}{LR_pC_a},$$

j is an imaginary unit and w is the angular frequency. The resonant frequency is obtained by the inflection point of the amplitude of the impedance equation. Therefore, the inflection point of the amplitude of the impedance equation is solved as:

$$\frac{d}{dw}|Z_{(jw)}| = \frac{d}{dw}\sqrt{\frac{a_{r2}^2 + (a_{r1}^2 - 2a_{r2})w^2 + w^4}{b_{r2}^2 + (b_{r1}w)^2}} = 0. \tag{10}$$

Assuming that the resonant frequency is the real and positive value, the resonant frequency R_f (Hz) is solved as:

$$R_f = \frac{w}{2\pi} = \frac{1}{2\pi}\sqrt{\frac{-b_{r2}^2 + \sqrt{a_{r2}^2b_{r1}^4 - a_{r1}^2b_{r1}^2b_{r2}^2 + 2a_{r2}b_{r1}^2b_{r2}^2 + b_{r4}^4}}{b_{r1}^2}}. \tag{11}$$

As a result of these calculations, the resonant frequency can be obtained.

2.4. *Experiment*

In order to evaluate the accuracy and the convergence characteristics of the identification, a computer simulation study was carried out. After the evaluation, this estimation was applied to an animal experiment.

2.4.1. Computer simulation study. In the computer simulation study, two physiologic models in state 1 and state 2 were prepared as in Table 1. In state 1, the physiologic parameters were set as $L = 0.025$ mmHg s^2/ml, $R_a = 0.05$ mmHg s/ml,

Table 1.
Summary of the preset physiologic parameters and the preset resonant frequency in the computer simulation study

	State 1	State 2
L	0.025	0.025
R_a	0.05	0.05
C_a	0.7	0.35
R_p	0.5	0.75
R_f	1.22	1.74

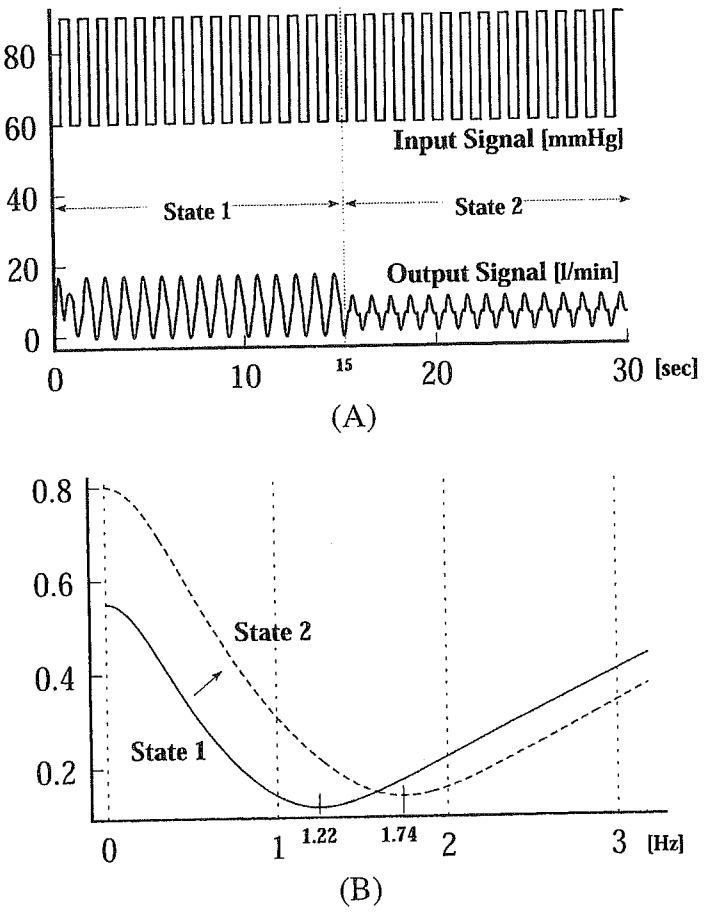

Figure 5. Results of the computer simulation study. (A) Input signal and the output signal. (B) Frequency characteristic of the preset model. (C) Results of the estimation of the physiologic parameters. (D) Results of the estimation of the resonant frequency.

$C_a = 0.7$ ml/mmHg and $R_p = 0.5$ mmHg s/ml. The resonant frequency was set as 1.22 Hz. In state 2, the physiologic parameters were set as $L = 0.025$ mmHg s^2/ml, $R_a = 0.05$ mmHg s/ml, $C_a = 0.35$ ml/mmHg and $R_p = 0.75$ mmHg s/ml. The resonant frequency was set as 1.74 Hz. To confirm the tracking performance against the variation of the physiologic parameters, the preset model was changed from state 1 to state 2, when t reached 15 s.

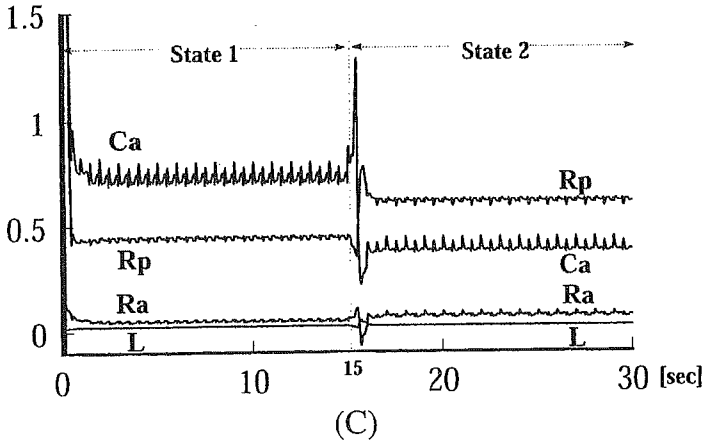

(C)

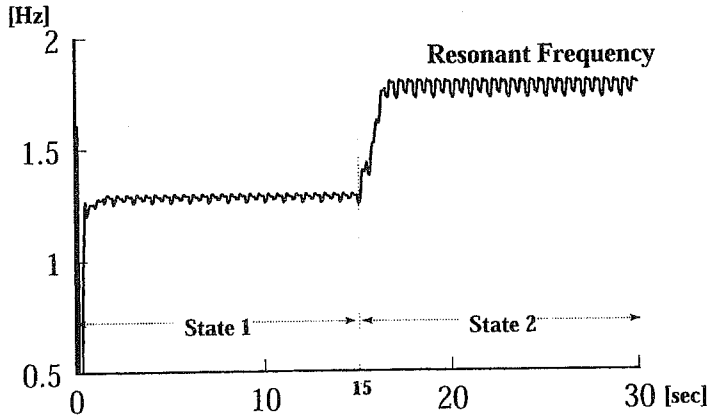

(D)

Figure 5. (Continued).

In this computer simulation study, considering the waveform of Aop, the input signal used a square wave and the output signal was calculated through the model by using the input signal. The input signal and output signal are shown in Fig. 5A. The frequency characteristics of the two models are shown in Fig. 5B.

2.4.2. Animal experiment. During the animal experiment using a 40-kg sheep, a magnetic suspension-type blood pump using direct drive [15] was attached as a LVAD. This artificial heart is shown in Fig. 6. The measured data were Aop measured by a pressure transducer (Nihon Kohden, Tokyo, Japan) at the root of the aorta and blood flow measured by an ultrasound tubing flow meter (Transonic Systems, Ithaca, NY, USA). This measured blood flow was the sum of the aortic flow measured at the ascending aorta and the pump flow measured at the outlet tube of the pump, and aortic flow and pump flow were measured at almost the same length from the connection point of the descending aorta and pump outlet tube. The waveforms of the measured data are shown in Fig. 7. The measured data were converted to digital data by an analog-to-digital (A/D) converter with 16 channels and 14-bit resolution (instruNet; GW Instruments, Somerville, MA, USA) and collected by the data acquisition server. The sampling time was 0.01 s.

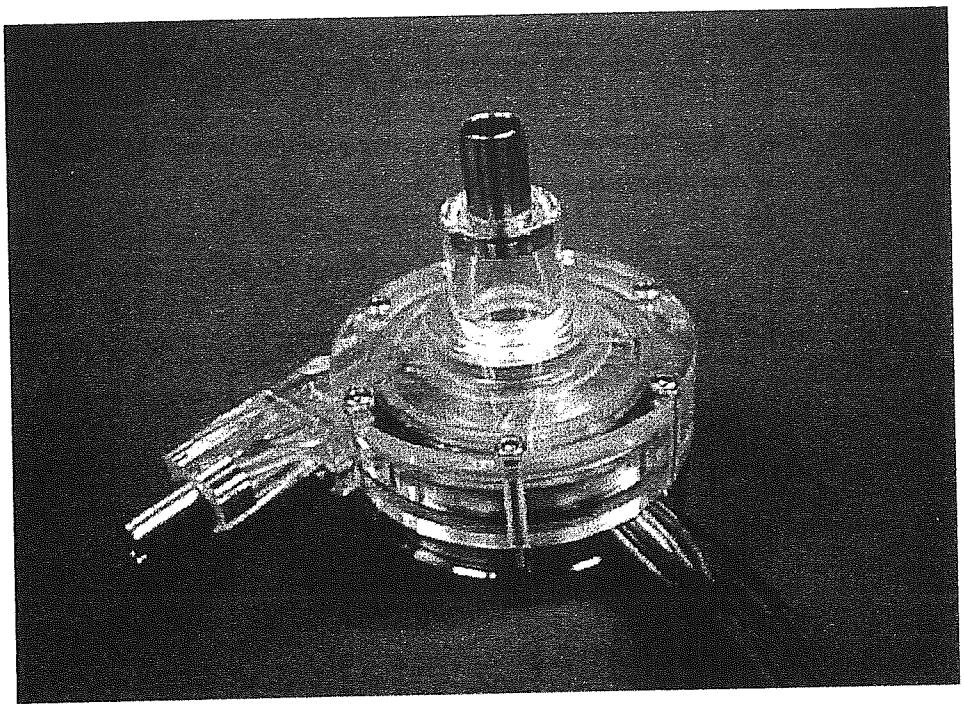

Figure 6. The magnetic suspension-type blood pump using a direct drive (AIST DD Series).

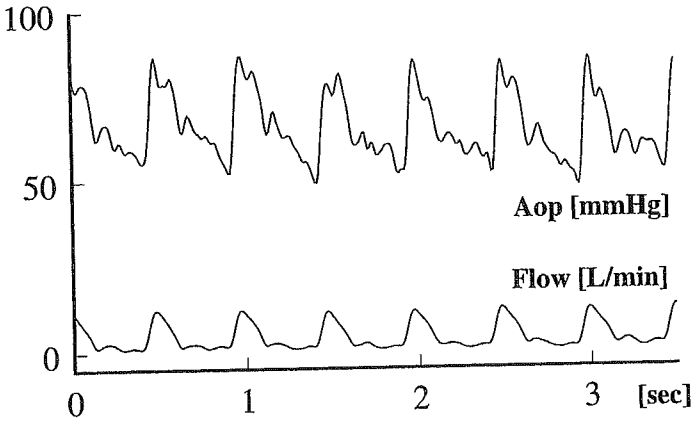

Figure 7. The Aop waveform used as the input signal and the blood flow waveform used as the output signal in the animal experiment.

3. RESULTS

3.1. Computer simulation study

Figure 5C and D shows the results of the computer simulation study for evaluation of the accuracy and convergence characteristic of the proposed estimation. Figure 5C shows the results of the estimation of the physiologic parameters. In state 1, the four identified physiologic parameters almost converged to the preset parameters: $L = 0.024$ mmHg s^2/ml, $R_a = 0.049$ mmHg s/ml, $C_a = 0.719$ ml/mmHg and $R_p = 0.45$ mmHg s/ml. The maximum error between the preset parameters and the mean identified parameters was almost 10% in R_p. In state 2, the

four identified physiologic parameters almost converged to the preset parameters: $L = 0.024$ mmHg s^2/ml, $R_a = 0.064$ mmHg s/ml, $C_a = 0.38$ ml/mmHg and $R_p = 0.62$ mmHg s/ml. The maximum error between the preset parameters and the mean identified parameters was almost 28% in R_a. Alhough the error ratio between the preset R_a and the identified R_a was large, the value of the error was small compared to the value of R_p. Thus the influence of this error was small. Figure 5D shows the results of the estimation of the resonant frequency. The resonant frequency also converged to the preset values: 1.27 Hz in state 1 and 1.76 Hz in state 2. The maximum error between the preset resonant frequency and the mean identified resonant frequency was almost 4%. With regard to the convergence characteristics, the identified physiologic parameters were tracked to the preset values within 1.0 s, regardless of the 25% changes of the preset physiologic model.

Therefore, in the computer simulation study, we confirmed the effectiveness of the proposed estimation to identify the physiologic parameters and the resonant frequency.

3.2. Animal experiment

Figures 8 and 9 show the results of the identification during the animal experiment. In this experiment, we focused on the terminal stage of the experiment, in which we could observe physiologic changes in particular.

Figure 8A shows the measured Aop and the measured blood flow. Upto postoperative day (POD) 70.5, the physiologic condition was stable (state 1). From POD 70.5 to POD 74, the physiologic condition was getting worse (state 2). After POD 74, the physiologic condition was at the terminal stage (state 3). Applying the proposed estimation method, the physiologic parameters and the resonant frequency were estimated shown as in Table 2.

Figure 8B and C shows the identified results of the physiologic parameters. The physiologic parameters were changed significantly during state 2. C_a was decreased from 0.5 to 0.2 mmHg/ml and R_p was increased from 0.4 to 1.0 mmHg s/ml. L and R_a were not changed compared to the variation of R_p and C_a.

Table 2.
Summary of the identified physiologic parameters and the identified resonant frequency during the animal experiment

	State 1	State 2	State 3
L	0.004	0.004	0.006
R_a	0.04	0.03	0.04
C_a	0.50	0.33	0.20
R_p	0.4	0.7	1.0
R_f	3.54	4.0	4.5

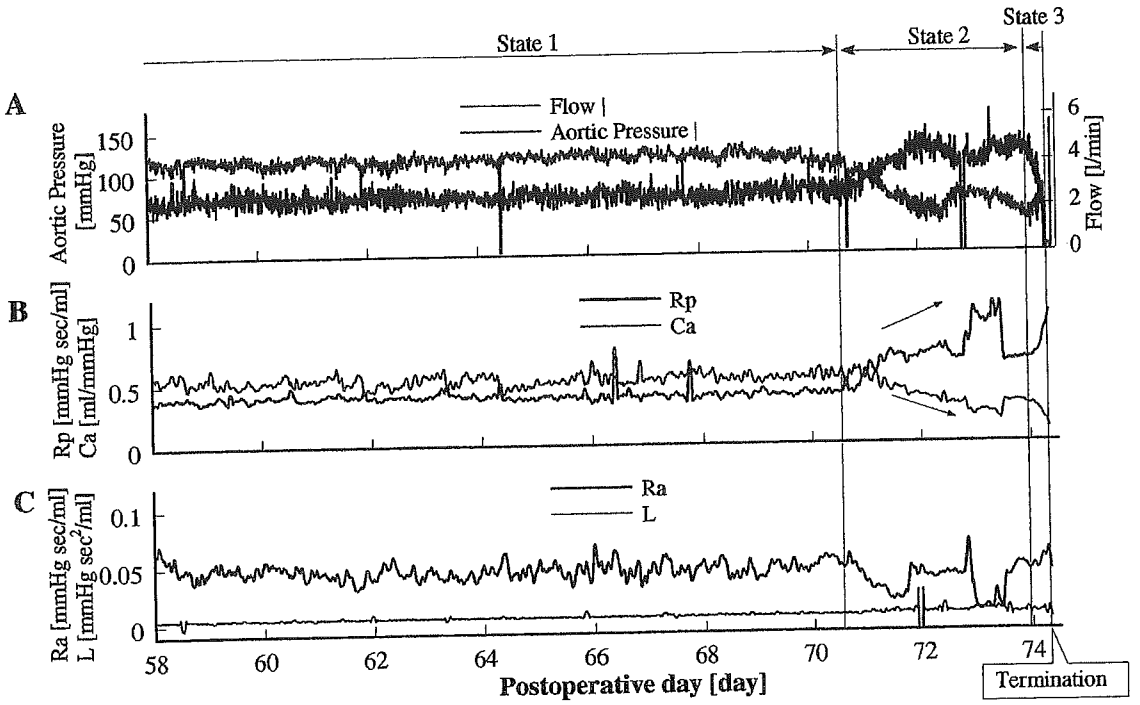

Figure 8. Estimated results of the identification during the animal experiment. (A) Measured Aop and measured blood flow. (B) Identified physiologic parameters: C_a and R_p. (C) Identified physiologic parameters: R_a and L.

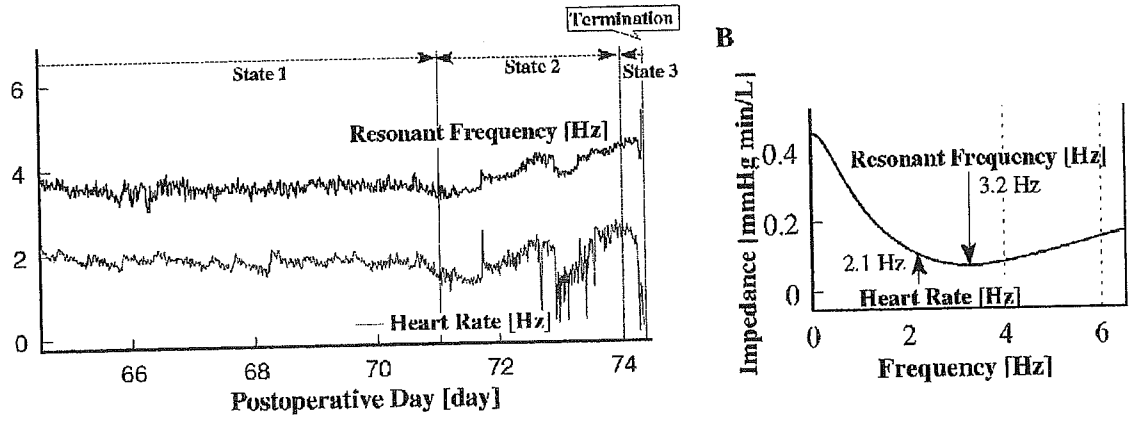

Figure 9. Estimated results of the resonant frequency during the animal experiment. (A) Comparison between the resonant frequency estimated by the proposed method and the measured heart rate. (B) Frequency characteristics.

Figure 9 shows the identified results of the resonant frequency. Figure 9A shows that the resonant frequency was increased from 3.35 to 4.54 Hz in the terminal stage. In Fig. 9B, since the resonant frequency of 3.2 Hz was near the heart rate of 2.1 Hz, we compared the resonant frequency with the heart rate. As a result, the heart rate was synchronized with the resonant frequency before POD 74. This result is shown in Fig. 9B.

4. DISCUSSION

During the animal experiment, both the physiologic parameters and the resonant frequency were estimated. From the definition of C_a and R_p, the aortic blood vessel became hard and the total peripheral blood vessels became narrow in the terminal stage. Around POD 73, even though the measured physiologic data did not change scientifically, the identified physiologic parameters changed in particular, as in the terminal stage. This physiologic change was not observed by the measured data. Using the changes in the identified physiologic parameters, we considered that in order to maintain the Aop, which was necessary to provide blood flow to the internal vital organs, especially the brain, the physiology increased the resistance and decreased the compliance in order to keep the Aop constant even if the blood flow was decreased.

As is shown by Fig. 9A, the heart rate related to the identified resonant frequency. Thus, we considered that the physiology adjusted the heart rate corresponding to the changes in the resonant frequency. Under the resonant frequency, the impedance was minimum and the heart could provide the maximum amplitude of the blood flow to the identified systemic circulation.

Thus, we estimated the physiologic strategy as the changes in the identified parameters online. In the terminal stage, the physiology controlled the physiologic impedance of the systemic circulation by changing the physiologic parameters and the heart rate, in order to maintain the Aop even if the blood flow produced by the diseased heart was reduced. As the identified physiologic parameters and resonant frequency reflect the physiologic strategy and unmeasured physiologic changes, we confirm that it is possible to produce effective medical care and therapeutic control using the robotic artificial heart for assisting and subsisting the cardiac functions.

5. CONCLUSIONS

We have proposed and developed a method for estimating the physiologic strategy based on a mathematical model for assisting and substituting the cardiac functions using online parameter identification by a robotic artificial heart. The physiologic strategy was estimated by the changes in the physiologic parameters of the systemic circulation identified from the mathematical model using online parameter identification with the δ operator and the resonant frequency calculated from the identified physiologic parameters. The effectiveness of this method could be confirmed in the computer simulation study. Using the physiologic parameters and the resonant frequency, we could estimate the physiologic strategy capable of adapting to the physiologic behaviors during the animal experiment. By expanding the proposed estimation of the physiologic strategy, it is possible to make enable effective medical care and therapeutic control by the robotic artificial heart capable of adapting to the physiologic behavior based on the changes in the identified physiologic parameters.

REFERENCES

1. Y. Nosé and K. Furukawa, Current status of the Gyro Centrifugal Blood Pump—development of the permanently implantable centrifugal blood pump as a biventricular assist device (NEDO Project), *Artif. Organs* **28**, 953–958 (2004).
2. C. Nojiri, T. Kijima, J. Maekawa, K. Horiuchi, T. Kido, T. Sugiyama, T. Mori, N. Sugiura, T. Asada, W. Umemura, T. Ozaki, M. Suzuki, T. Akamatsu, S. Westaby, T. Katsumata and S. Saito, Development status of Terumo implantable left ventricular assist system, *Artif. Organs* **25**, 411–413 (2001).
3. R. D. Dowling, L. A. Gray Jr, S. W. Etoch, H. Laks, D. Marelli, L. Samuels, J. Entwistle, G. Couper, G. J. Vlahakes and O. H. Frazier, Initial experience with the AbioCor implantable replacement heart system, *J. Thorac. Cardiovasc. Surg.* **127**, 131–141 (2004).
4. G. M. Wieselthaler, H. Schima and E. Wolner, Special considerations on the implantation technique for the MicroMed-DeBakey ventricular assist device axial pump, *Ann. Thorac. Surg.* **76**, 2109–2111 (2003).
5. K. Nakata, M. Yoshikawa, T. Takano, Y. Sankai, G. Ohtsuka, J. Glueck, A. Fujisawa, K. Makinouchi, M. Yokokawa, S. Nosaka and Y. Nosé, Control system for an implantable rotary blood pump, *Ann. Thorac. Cardiovasc. Surg.* **6**, 242–246 (2000).
6. H. Yamagishi, Y. Sankai, T. Yamane, T. Jikuya and T. Tsutsui, Development of built-in-type and bloodless sensor system for smart artificial heart, *ASAIO J.* **49**, 265–270 (2001).
7. Y. Sankai, H. Koguchi, R. Takiya, R. Kosaka, T. Tsutsui, T. Jikuya and T. Yamane, Bio-telemetry system and non-invasive sensors for smart artificial heart (SAH), *ASAIO J. Abstr.* **46**, 205 (2000).
8. R. Kosaka, Y. Sankai, R. Takiya, T. Jikuya, T. Yamane and T. Tsutsui, Tsukuba remote monitoring system for continuous-flow artificial heart, *Artif. Organs* **27**, 897–906 (2003).
9. B. A. Deswysen, Parameter estimation of a simple model of the left ventricle and of the systemic vascular bed, with particular attention to the physical meaning of the left ventricular parameters, *IEEE Trans. Biomed. Engng* **24**, 29–38 (1977).
10. A. C. Guyton, T. G. Coleman, A. V. Cowley Jr, K. W. Scheel, R. D. Manning Jr and R. A. Norman Jr, Arterial pressure regulation. Overriding dominance of the kidneys in long-term regulation and in hypertension, *Am. J. Med.* **52**, 584–594 (1972).
11. M. K. Sharp and R. K. Dharmalingam, Development of a hydraulic model of the human systemic circulation, *ASAIO J.* **45**, 535–540 (1999).
12. S. Kitamori, Unified expression and approach to continuous-and discrete-time control, *J. SICE* **22**, 599–605 (1983).
13. T. Mita, Digital optimal control, *J. SICE* **27**, 1058–1064 (1988).
14. G. C. Goodwin, R. L. Leal, D. Q. Mayne and R. H. Middleton, Rapprochement between continuous and discrete model reference adaptive control, *Automatica* **22**, 199–207 (1986).
15. T. Yamane and M. Nishida, Fundamental characteristics of a magnetic-suspension-type-blood pump using a direct-drive, *Jpn. J. Artif. Organs* **26**, 386–389 (1997).

ABOUT THE AUTHORS

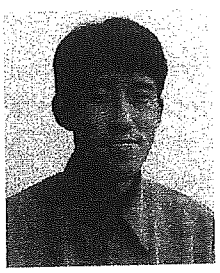

Ryo Kosaka received the BE and ME degrees in Engineering Systems from the University of Tsukuba, Japan in 2000 and 2002, respectively. Currently he is named a Japan Society for the Promotion of Science (JSPS) Fellow, Doctoral student in the Institute of Systems and Information Engineering, University of Tsukuba, Japan. His research interests include the next generations of artificial hearts as related fields of cybernics. He received awards from the International Society for Rotary Blood Pump in 2002 and 2003. He is a member of the ISRBP, JSAO and ASAIO.

Yoshiyuki Sankai received the PhD degree in engineering from the University of Tsukuba, Japan in 1987. He was a JSPS research fellow, Assistant Professor, Associate Professor and Professor of Institute of Systems and Engineering in the University of Tsukuba, and a Visiting Professor at Baylor College of Medicine in USA. Currently, he is a professor and director of the prioritized research area 'New Robotics Frontier: Cybernetics', Graduate School of System and Information Engineering in University of Tsukuba, Japan. His research interests include Robot Suit HAL (Hybrid Assistive Limb), the next generation of artificial heart, humanoid Control, Bio-Medicine Science, Network Medicine as related fields of Cybernetics. He received a Grant of the Japanese Society for Artificial Organs (JSAO), Awards from the American Society for Artificial Organs, International Society for Artificial Organs, International Society for Rotary Blood Pump with his students and so on. He was/is a president of Japan Society of Embolus Detection and Treatment, a chair of *International Journal of the Robotics Society of Japan*, a member of the Awards Committee in the Robotics Society of Japan and Japan Society of Mechanical Engineers, and executive editor of Vascular Lab., an executive board member of Robotics Society of Japan, a founder and a chairman of CYBERDYNE Inc.

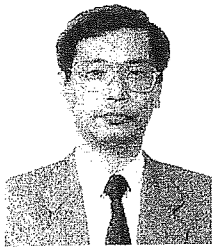

Takashi Yamane received the PhD degree in aeronautics from the University of Tokyo in 1980. Immediately he joined the Mechanical Engineering Laboratory, Ministry of International Trade and Industry. In 1998 he received the Prize for Scientific Effort from the Mechanical Engineering Laboratory. Since 2001 he has been Deputy Director at the Institute for Human Science and Biomedical Engineering, National Institute of Advanced Industrial Science and Technology. He is now a Trustee of the Society of Life Support Technology and Chair of the Medical Electromagnetic Drivers Committee, Institute of Electrical Engineers of Japan.

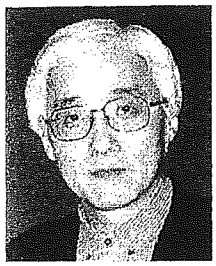

Tatsuo Tsutsui received the MB in 1975 from Tohoku University, Sendai, Japan, and the PhD degree in Medical Sciences in 1983 after his training in cardiovascular surgery at the Heart Institute of Japan, Tokyo Women's Medical College, Tokyo, Japan. From 1985 to 1986, he was a Research Fellow at the Department of Artificial Organs, Cleveland Clinic, Cleveland, USA. He received the Fellowship Award in 1986 from the American Society for Artificial Internal Organs. His current research interests include physiological research in the application of artificial hearts and biological circulatory control systems. He is currently Associate Professor in the Institute of Clinical Medicine, University of Tsukuba, and Director of the Department of Critical Care Medicine, Tsukuba University Hospital.

Advanced Robotics, Vol. 19, No. 7, pp. 773–795 (2005)

Also available online - www.vsppub.com

Full paper

Virtual impedance adjustment in unconstrained motion for an exoskeletal robot assisting the lower limb

SUWOONG LEE * and YOSHIYUKI SANKAI

Graduate School of Systems and Information Engineering, University of Tsukuba, 1-1-1 Tennodai, Tsukuba, Ibaraki 305-8573, Japan

Received 11 May 2004; accepted 12 August 2004

Abstract—The objective of this paper is to establish the criteria for adjusting the virtual impedance of an exoskeletal robot for the lower limb in order to minimize the operator's physical stress in unconstrained motion. The exoskeletal robot HAL (Hybrid Assistive Limb)-3 which we developed for assisting the motor function of the lower limb was used for experiments in this research. To accomplish the objective (i) the physical parameters around the joint of HAL-3 were identified and (ii) the relationships between the virtual impedance values and the physical stress of operators were examined through experiments for swinging motions of the lower leg. The physical stress was evaluated with myoelectricity, the musculoskeletal moment of the operator and the operator's feelings during the experimental motion. As a result, we found that the physical stress tended to decline with the decrease of virtual inertia and virtual Coulomb friction, and to increase slightly with the decrease of virtual gravitational moment. The decrease of virtual viscous friction made the physical stress increase gradually after it declined to a trough during the positive virtual viscous friction. Based on the results, we could establish the criteria for adjusting the virtual impedance for minimizing the operator's physical stress in unconstrained motion.

Keywords: Assist; virtual impedance; physical stress; parameter identification; unconstrained motion.

1. INTRODUCTION

Exoskeletal robot suits aimed at supporting the works of labor or the movements of aged persons have the ideal form to assist a human's motion, and they are expected to be used in many fields such as labor-intensive industries, welfare and medicine. In particular, it is likely that exoskeletal robots for assisting the motor function of the lower limb will be very useful for supporting a human's locomotion in the work area or living space [1–3].

*To whom correspondence should be addressed. E-mail: lee@golem.kz.tsukuba.ac.jp

imental setups and the evaluation methods for the experimental results. Section 4 examines and evaluates the relationships between the virtual impedance values and the physical stress of the operators through experiments for unconstrained motions of the lower leg. Section 5 discusses the experimental results.

2. HAL-3

2.1. Hardware configuration of HAL-3

Figures 2 and 3 show the hardware configuration and the structure of the exoskeleton-type power assist system HAL-3 used in the experiments. It consists of a three-link, two-joint mechanism corresponding to the human lower limb. The joints of the exoskeleton are powered by actuators composed of DC servo motors and gears, and controlled in torque control mode according to an operational signal from a control computer. Mechanical constraints attached to joints keep the joint angle of the exoskeleton within human anthropometric boundaries. Potentiometers are attached to the center of the exoskeletal joint axes so as to measure the angle of joints and force sensors are mounted at the exoskeletal frame to measure the force applied by the operator to the exoskeleton of HAL-3. Myoelectric electrodes are attached on the operator's skin for measuring the myoelectric signal of the flexor and extensor muscles of the joint. In this paper, experiments focused on the motion

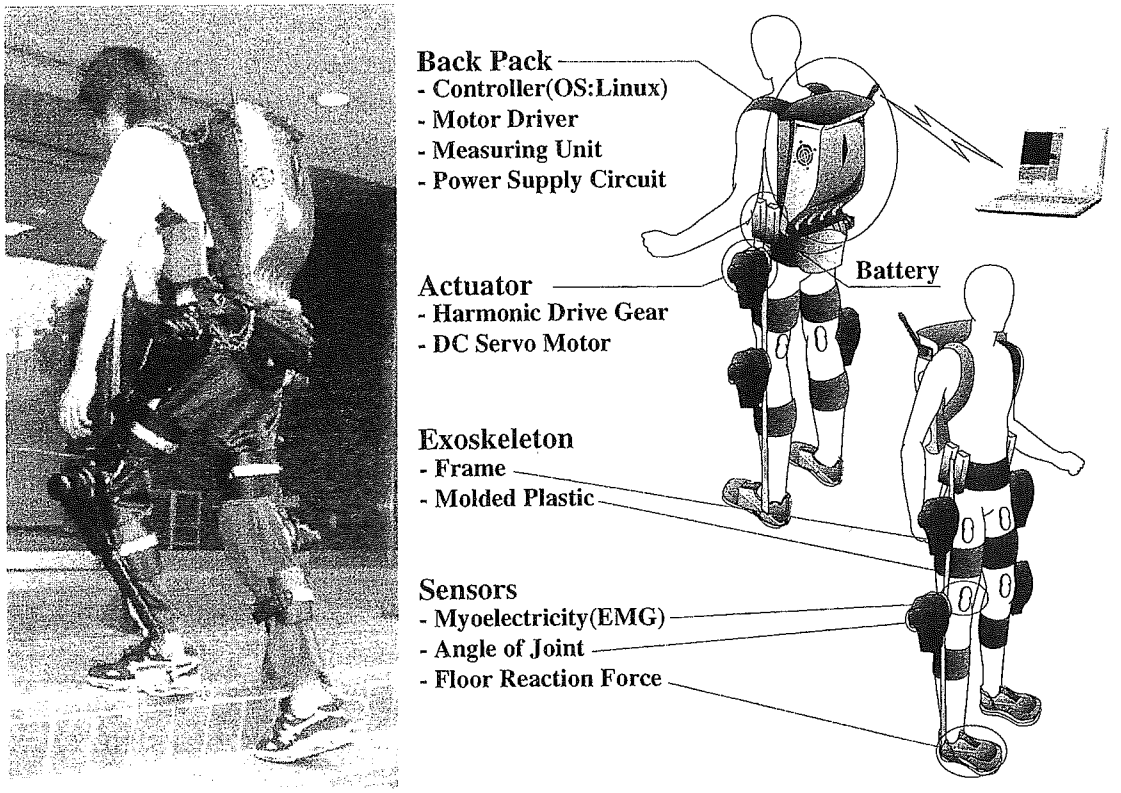

Figure 2. HAL-3.

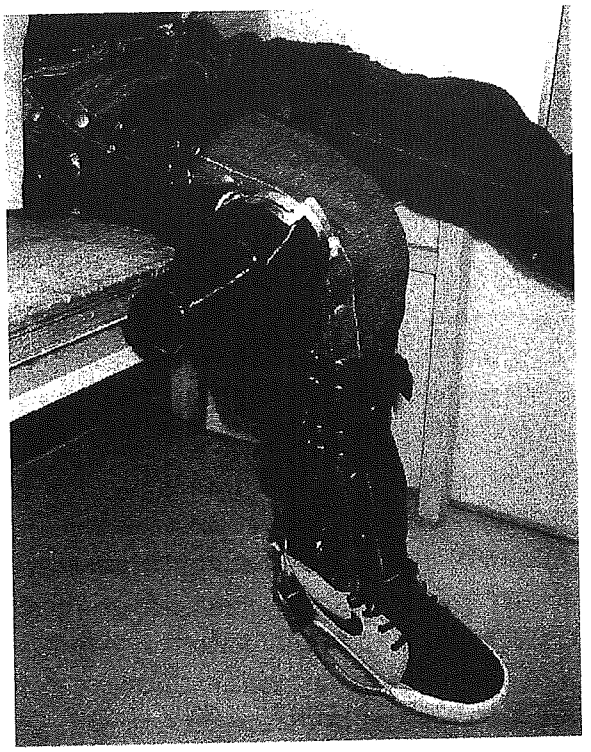

Figure 3. Exoskeletal structure of HAL-3.

around the knee joint were carried out, so the angle of the knee joint, the force applied by the operator's lower thigh, and the myoelectricity at the biceps femoris as flexor muscle and vastus medialis as extensor muscle of the knee joint were measured as the required data for the evaluation of the experimental results. The measured data were fed to the control computer at a sampling rate of 1 kHz.

2.2. *Identification of dynamic parameters of the exoskeleton of HAL-3*

The dynamic parameters of HAL-3's exoskeleton, such as inertia moment, viscous friction coefficient, gravitational moment and Coulomb friction, were identified before the experiments in order to adjust the virtual impedance. The motion equation around the knee joint of the exoskeleton is expressed as (1):

$$I_{\mathrm{h}}\frac{\mathrm{d}^2\theta(t)}{\mathrm{d}t^2} + D_{\mathrm{h}}\frac{\mathrm{d}\theta(t)}{\mathrm{d}t} + M_{\mathrm{h}}gl_{\mathrm{h}}\sin\theta(t) + C_{\mathrm{a}}\,\mathrm{sign}\left(\frac{\mathrm{d}\theta(t)}{\mathrm{d}t}\right) = \tau_{\mathrm{a}}(t), \qquad (1)$$

where I_{h}, D_{h}, $M_{\mathrm{h}}gl_{\mathrm{h}}$ and C_{a} represent inertia moment, viscous friction coefficient, gravitational moment and Coulomb friction around the knee joint of the exoskeleton, respectively, $\theta(t)$ is the angle of the knee joint, $\mathrm{sign}(\mathrm{d}\theta(t)/\mathrm{d}t)$ is the sign of the angular velocity, and $\tau_{\mathrm{a}}(t)$ is the torque generated by the actuator. Equation (1) can be expressed by:

$$\Omega(t)X = \tau_{\mathrm{a}}(t), \qquad (2)$$

where:

$$\Omega(t) = \left[\frac{\mathrm{d}^2\theta(t)}{\mathrm{d}t^2} \frac{\mathrm{d}\theta(t)}{\mathrm{d}t} \sin\theta(t) \operatorname{sign}\left(\frac{\mathrm{d}\theta(t)}{\mathrm{d}t} \right) \right], \tag{3}$$

$$X = [I_\mathrm{h} \;\; D_\mathrm{h} \;\; M_\mathrm{h} g l_\mathrm{h} \;\; C_\mathrm{a}]^\mathrm{T}. \tag{4}$$

When $\hat{X}(t)$ and ε represent the matrix of unknown parameters to be identified and the error between estimated torque calculated with $\hat{X}(t)$ and measured torque, respectively, $\tau_\mathrm{a}(t)$ is expressed as:

$$\tau_\mathrm{a}(t) = \Omega(t)\hat{X}(t) + \varepsilon = \hat{\tau}_\mathrm{a}(t) + \varepsilon, \tag{5}$$

where $\hat{\tau}_\mathrm{a}(t)$ is estimated torque. Based on the condition to minimize the squared error ε^2 as:

$$\frac{\partial J(t)}{\partial \hat{X}(t)} = 0, \tag{6}$$

$$J(t) = \varepsilon^\mathrm{T}\varepsilon = \left(\tau_\mathrm{a}(t) - \Omega(t)\hat{X}(t)\right)^\mathrm{T}\left(\tau_\mathrm{a}(t) - \Omega(t)\hat{X}(t)\right), \tag{7}$$

unknown parameters $\hat{X}(t)$ are found as (8):

$$\hat{X}(t) = \left(\Omega(t)^\mathrm{T}\Omega(t)\right)^{-1}\left(\Omega(t)^\mathrm{T}\tau_\mathrm{a}(t)\right). \tag{8}$$

In the experiments for parameter identification, the actuator was driven in sinusoidal patterns with frequencies of 0.33, 0.67 and 1.33 Hz, which gave better experimental results in the preceding trials [7]. Angular acceleration and angular velocity were calculated from the smoothed difference values of angle data. In total, 10 experiments were performed, and parameters were found as the mean values of experimental results. Table 1 summarizes the mean values of the identified parameters of HAL-3's exoskeleton.

Table 1.
Identified parameters around the knee joint of the exoskeleton (means ± SD of 10 trials)

Parameters	Identified values
Inertia moment (kg m^2)	0.17 ± 0.001
Viscous coeff. (N m/(rad/s))	3.13 ± 0.08
Gravitational moment (N m)	3.31 ± 0.004
Coulomb friction (N m)	0.57 ± 0.02

3. EXPERIMENTAL DETAILS

In this paper, the experiments were performed in two steps: (i) the virtual impedance values around the knee joint of HAL-3 were adjusted individually and (ii) the virtual impedance values were adjusted properly based on former experimental results. The relationships between the physical stress and the virtual impedance were then analyzed.

3.1. Experimental system composed of the operator and HAL-3

The equation of motion of the operator's lower thigh including the exoskeleton of HAL-3 can be expressed as:

$$(I_s + I_h)\frac{d^2\theta(t)}{dt^2} + (D_s(u(t)) + D_h)\frac{d\theta(t)}{dt} + (M_s g l_s + M_h g l_h)\sin\theta(t) + C_a \operatorname{sign}\left(\frac{d\theta(t)}{dt}\right) = \tau_a(t) + \tau_m(t), \tag{9}$$

where I_s, D_s and $M_s g l_s$ represent inertia moment, viscous friction coefficient and gravitational moment around the knee joint of the operator, respectively, $u(t)$ is the muscle activation at the knee joint of the operator, and $\tau_m(t)$ is the torque generated by the muscles (musculoskeletal moment). Note that I_h, D_h, $M_h g l_h$ and C_a are previously identified parameters (Table 1). In (9), we assumed the stiffness by the operator's muscles is very small in comparison with other parameters. When compensating torque is generated by actuator as:

$$\tau_a(t) = (I_h - I_v)\frac{d^2\theta(t)}{dt^2} + (D_h - D_v)\frac{d\theta(t)}{dt} + (M_h - M_v) g l_h \sin\theta + (C_a - C_v)\operatorname{sign}\left(\frac{d\theta(t)}{dt}\right). \tag{10}$$

Substituting $\tau_a(t)$ from (10) into (9) results in the experimental motion expressed as (11):

$$(I_s + I_v)\frac{d^2\theta(t)}{dt^2} + (D_s(u(t)) + D_v)\frac{d\theta(t)}{dt} + (M_s g l_s + M_v g l_h)\sin\theta(t) + C_v \operatorname{sign}\left(\frac{d\theta(t)}{dt}\right) = \tau_m(t), \tag{11}$$

where I_v, D_v, $M_v g l_h$ and C_v represent virtual impedance which can be chosen by the experimenter.

Figure 4 depicts the configuration of the overall experimental system. The operators were seated on a firm platform so as to be able to swing his/her lower thigh stably for a long time. An experimenter could browse the measured data such as the angle of the joint and adjust the experimental settings with a palm-top computer through a wireless LAN.

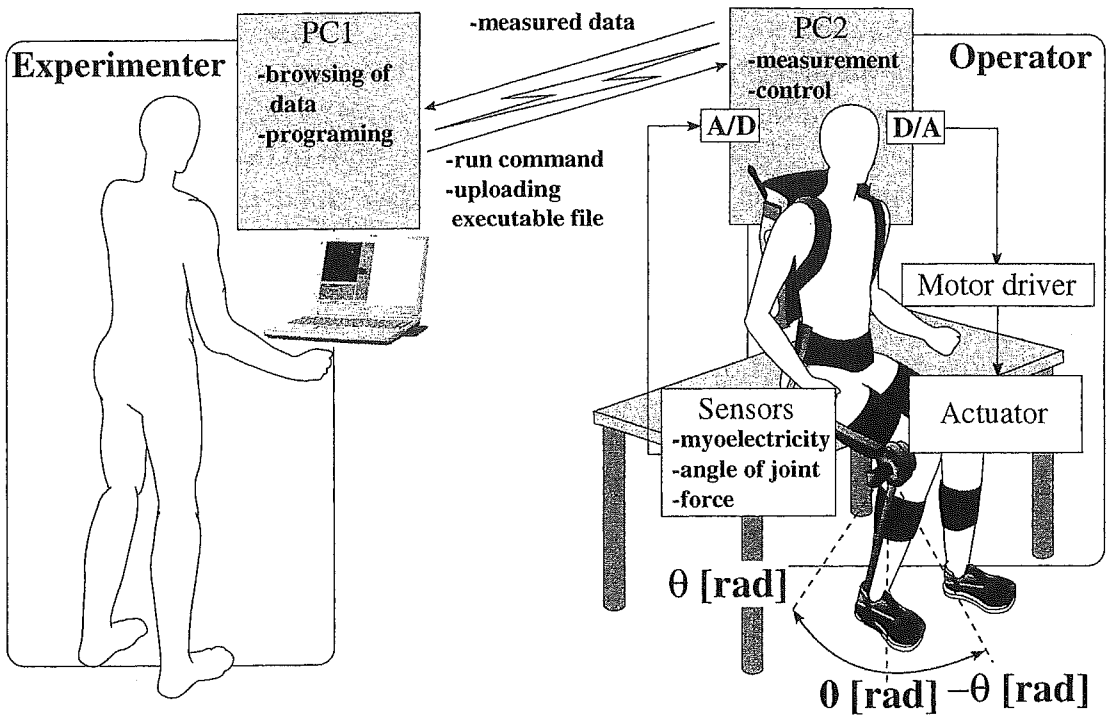

Figure 4. Schematic overview of the experimental system.

Table 2.
The set values of the virtual impedance

Virtual impedance	Set value	Tolerance
I_v (kg m^2)	0.170 to −0.020	−0.020
D_v (N m/(rad/s))	3.128 to −0.782	−0.391
$M_v g l_h$ (N m)	3.310 to −0.828	−0.414
C_v (N m)	0.560 to −0.140	−0.070

3.2. Settings of experimental condition

In the experiments, the operators were instructed to swing their lower thigh according to the same boundary values and frequency so that we could evaluate unconstrained motions under the same conditions. The boundary values of the knee joint angle and frequency for unconstrained motion were set to ±0.5 rad and 1 Hz, respectively [7]. Figure 5 depicts the myoelectricity at the flexor and extensor muscles, the musculoskeletal moment calculated based on the measured force, and the angle of the knee joint measured in the experiments.

Experiments were performed in two steps. In the first step, the virtual impedance around the knee joint of HAL-3 was adjusted individually in 10 steps as shown in Table 2. The operator swung his/her lower thigh for 10 min, and the experimental trials were performed in sets of 10 steps 5 times for an operator and for virtual impedance. In the second step, the virtual impedance was adjusted properly at once,

based on the results of the former experiments, and the operators swung his/her lower thigh as in the first experiments.

The operators were three unimpaired persons who were 28 (A), 22 (B) and 21 (C) years old, respectively. They had break times between trials so that muscular fatigue did not have an influence on the motions of the operators and the myoelectricity [8].

3.3. Method of evaluation of the experimental results

It is likely that the method of evaluation of the the experimental results should include not merely objective, but also subjective factors since the overall experimental system is composed of a robot and a human.

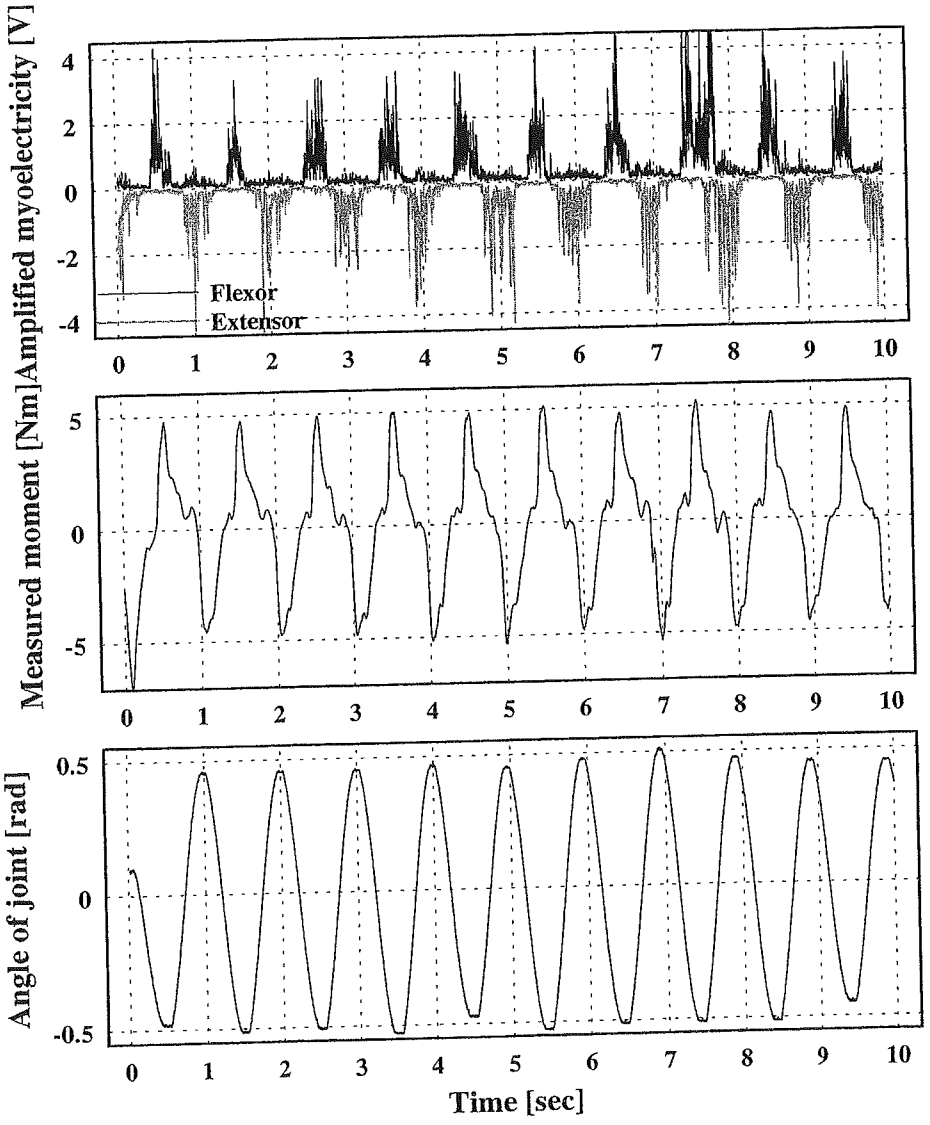

Figure 5. Data of the experimental motion (myoelectricity at the flexor and extensor muscles, musculoskeletal moment applied to exoskeleton and angle of joint).